Astron. Astrophys. 336, 662–666 (1998)

ASTRONOMY AND ASTROPHYSICS

Mid-IR mapping of the region of N 4 in the Large Magellanic Cloud with ISOCAM⋆

A. Contursi[1], J. Lequeux[1], M. Hanus[1], M. Heydari-Malayeri[1], C. Bonoli[2], A. Bosma[3], F. Boulanger[4], D. Cesarsky[4], S. Madden[5], M. Sauvage[5], D. Tran[5], and L. Vigroux[5]

[1] Observatoire de Paris, 61 Av. de l'Observatoire, F-75014 Paris, France
[2] Osservatorio Astronomico, Viccolo Osservatorio, I-35122 Padova, Italy
[3] Observatoire de Marseille, 2 Place Le Verrier, F-13248 Marseille Cedex 04, France
[4] Institut d'Astrophysique Spatiale, Bat. 121, Université Paris XI, F-91450 Orsay Cedex, France
[5] SAp/DAPNIA/DSM, CEA-Saclay, F-91191 Gif-sur-Yvette Cedex, France

Received 18 June 1997 / Accepted 24 September 1997

Abstract. We present images of the N 4 region in the Large Magellanic Cloud obtained with ISOCAM on board ISO through broad band filters centered at 6.75 and 15 μm. Far from the three H II regions contained in the map, the emission at both wavelengths is due to the Unidentified Infrared Bands and associated continuum and originates in the external layers of a molecular cloud complex. The ratio between the intensities at 15 and 6.75 μm is $\simeq$ 0.6–0.7 comparable to the 0.55–0.85 ratio found in our Galaxy. Closer to the H II regions, this ratio increases when the ultraviolet radiation density reaches $\simeq 10^3$ times the radiation density near the Sun, due to the contribution of very small grains to the flux near 15 μm. The emission at both wavelengths is maximum in the direction of an interface between the main H II region N 4A and the molecular cloud, a region very similar to the classical interface of M 17 in our Galaxy. We have detected at both mid-IR wavelengths the emission of a M supergiant present in the field.

Key words: ISM: N 4 (LMC) – Magellanic clouds – infrared: ISM: continuum – infrared: ISM: lines and bands – ISM: clouds – ISM: H II regions

1. Introduction

N 4 (Henize 1956), also designated as DEM 8 (Davies et al. 1976) is a complex of H II regions in the north-west part of the Large Magellanic Cloud (LMC). These H II regions and the associated molecular complex have been comprehensively studied by Heydari-Malayeri & Lecavelier des Etangs (1994). They make a relatively isolated, simple structure of about $4'$ in size, well suited for mapping with the mid-infrared camera ISOCAM on board the Infrared Space Observatory (ISO). In this paper, we present maps of the whole region obtained with $6'' \times 6''$ pixels in two broad band filters LW2 and LW3, covering respectively the spectral ranges 5.5–8.5 and 12.0–17.0 μm. At least in our Galaxy, the emission in the LW2 filter is dominated by the Unidentified Infrared Bands (UIBs) at 6.2, 7.7 and 8.6 μm. That in the LW3 filter is partly continuum from the same carriers as the UIBs (often called Polycyclic Aromatic Hydrocarbons or PAHs although their exact nature is not known). If the radiation field is sufficiently large there is also a contribution from Very Small Grains (VSGs), perhaps made of graphite, heated closer to thermal equilibrium than the UIB carriers which are heated only transiently by single photons (Désert et al. 1990; Dwek et al. 1997). There are also some contributions of the UIB at 12.7 μm and possibly of the fine-structure lines [Ne II] 12.8 μm and [Ne III] 15.5 μm if there is ionized gas along the line of sight, but these contributions seem small in general. For a discussion of these properties, see Cesarsky et al. (1996a) and Cesarsky et al. (1996b). Consequently, observations with the LW2 and LW3 filters provide the opportunity to investigate the distribution of PAH and VSG emission in molecular–H II region complexes such as those of N 4. The main interest of a study of a LMC complex is that the properties of interstellar grains are known to differ from those in our Galaxy, as shown by observations with IRAS (Sauvage et al. 1990), probably due to differences in heavy-element abundances or/and in the ultraviolet radiation field.

In Sect. 2, we describe the observations and the reductions; Sect. 3 discusses the filter maps and the LW3/LW2 color map; Sect. 4 contains the conclusions.

2. Observations and reductions

A $6.4' \times 6.4'$ map centered on the main H II region N 4A was obtained in each of the LW2 and LW3 filters, with $6'' \times 6''$ pixels. The 32×32 pixel long-wavelength camera of ISOCAM was used to make a square 3×3-step raster map with a shift (then

Send offprint requests to: lequeux@mesioa.obspm.fr

⋆ Based on observations with ISO, an ESA project with instruments funded by ESA member states (especially the PI countries: France, Germany, the Netherlands and the United Kingdom) and with the participation of ISAS and NASA.

overlap) of 16 pixels between successive positions. The single read-out integration time was 2 seconds. The 25 and 34 first reads-out obtained with the LW2 and the LW3 filter respectively were eliminated for the first step of the raster map in order to insure stabilization of the detectors, which show memory effects of their previous history. The useful total integration time at 7 and 15 μm respectively was 618 and 584 seconds. The map at each position was dark-current subtracted and flat-field ed in the usual way. Then an automatic software was used to detect and eliminate the parts of the records affected by glitches due to the impact of charged particles, and also to correct for the transient response of the detectors when submitted to changes in incident flux. Corrections for field distortion have been applied to images in both filters before combining the images of each raster, providing a better sensitivity on the final maps. A second-order flat-field correction was finally used to match the levels on contiguous edges of the elementary maps of the raster. This correction is only a few per cent and affects the photometry in a negligible way.

The images were calibrated using the library of calibration files associated with version 4.3 of the off-line software in Villafranca, Spain. One should be aware that a definitive reduction of the ISOCAM images is not yet possible. At the present stage, imperfect correction for the transient behavior of the detectors is likely to yield systematic errors in the flux determinations up to 30%. We cannot at this stage assign errors to the fluxes or flux ratios.

3. ISO filter maps of the region of N 4

Fig. 1 shows the LW3 (15 μm) map superimposed on the Hα image obtained by Heydari-Malayeri & Lecavelier des Etangs (1994). This image (their Fig. 1a) shows the bright H II region N 4A. N 4A is presumably ionized by a pair of central stars, not visible in this saturated image. 1′ to the NE is the fainter H II region N 4B with a conspicuous central star. 1′ to the NW of N 4A is the bright star WOH 53 (Westerlund et al. 1981), a M supergiant belonging to the Large Magellanic Cloud (Rebeirot et al. 1983). The relatively faint, filamentary H II region N 4C is located 2.5′ E of N 4A, outside the Hα map. A strong emission is seen associated with N 4A but displaced to the NE. There is a fainter emission in the direction of N 4B and of N 4C.

Fig. 2 shows the LW2 (6.75 μm) map, this time superimposed on the Digital Sky Survey image. The sensitivity is higher in this map, which displays extended structure not seen in the LW3 map. Emission is seen associated with N 4A and N 4C. The emission associated to N 4B is present but fainter than the 3 r.m.s noise level (per pixel): it is not displayed in the figure.

The outlines of the LW2 map coincide rather well with the ^{12}CO(1–0) map obtained at 43″ resolution (Fig. 8a of Heydari-Malayeri & Lecavelier des Etangs 1994), as it can be seen on Fig. 3. Unfortunately the CO map is not sufficiently extended to see if there is CO coinciding with the PAH emission in the easternmost part of the LW2 map. There is a strong emission in the LW2 filter in the direction of WOH 53; it will be discussed later. Another point source in the LW2 image at α(2000)= 04^h 52^m 02^s and δ(2000)= -66^0 52′ 38″ is identified with a star in the ESO on-line Digital Sky Survey (DSS). The absence of photometry for this object does not allow us to further investigate on the origin of its 7 μm emission. Both stars have been used to re-center the LW2 map on the DSS, while the LW3 map was centered only on WOH 53; its orientation was assumed to be correct, which is usually the case for such ISO observations. The relative position uncertainty between the two maps is of the order of half a pixel (3 arc seconds).

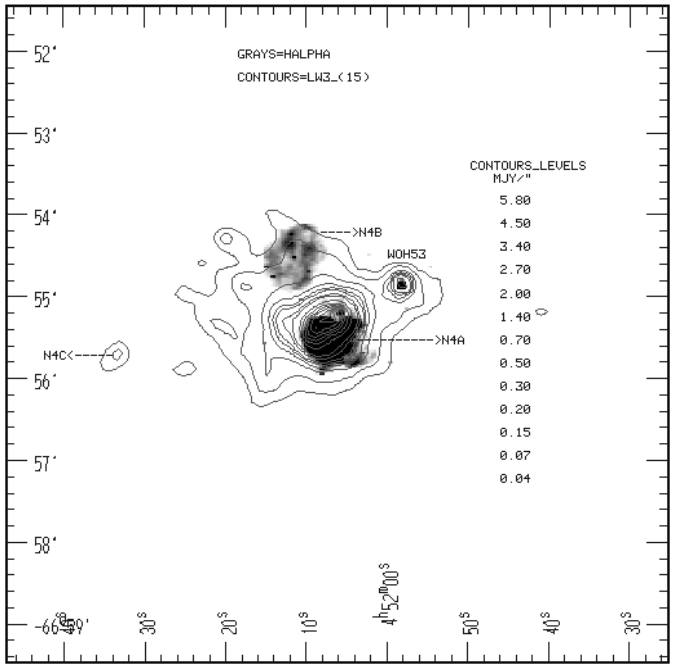

Fig. 1. Map of the N 4 region in the LW3 filter centered at 15 μm (contours) superimposed on an Hα image. The coordinates are J2000. The "source" at α= 04^h 52^m 20^s and δ= -66^0 54.4′ is an artefact due to the remanence of the detector. The H II region N 4A is located at the center of the figure. 1′ to the NNE is the fainter H II region N 4B with its conspicuous central star. 1′ to the WNW of N 4A is the bright star WOH 53, one of the brightest M supergiants in the LMC (Westerlund et al. 1981). The relatively faint, filamentary H II region N 4C is located 2.5′ E of N 4A, outside the Hα map. It corresponds to the easternmost peak of the ISO map. Contour levels are in mJy per square arcsecond. The first contour is at 3 r.m.s. noise level.

For the bright M2 supergiant WOH 53, (Westerlund et al. 1981) we measure a flux density of approximately 0.47 Jy and 0.14 Jy at 6.75 and 15 μm respectively. Together with the optical

agnitudes of the star (B=13.3, V=11.6, R=9.9, I=7.8: Rebeirot et al. 1983; Westerlund et al. 1981), these fluxes indicate an approximate effective temperature of 3000 K, corresponding to a M supergiant with no circumstellar envelope, or to a hotter supergiant with some circumstellar emission. A discussion of the properties of this star requires a deeper optical study.

4. Discussion

The ratio of intensities in the LW3 and LW2 filters (the LW3/LW2 color map) is displayed in Fig. 4. Due to the differ-

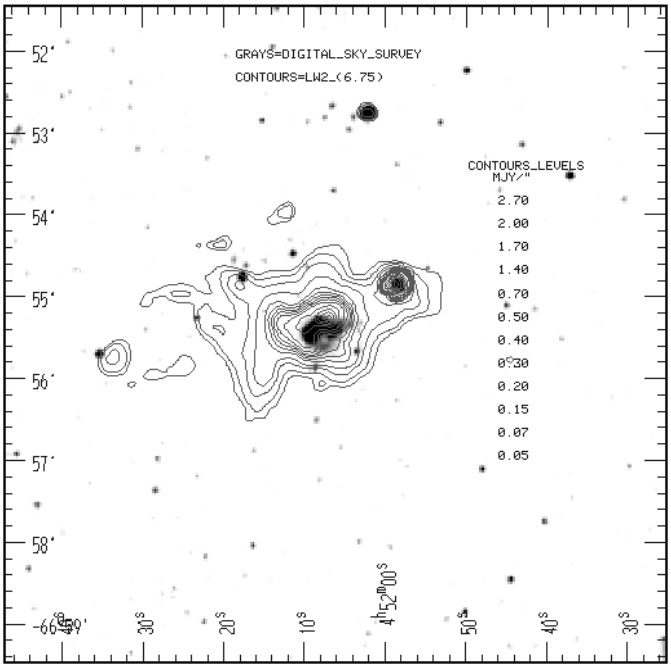

Fig. 2. Map of the N 4 region in the LW2 filter centered at 6.75 μm (contours) superimposed on the Digitized Sky Survey image. The coordinates are J2000. The "source" at α= 04^h 52^m 20^s and δ= -66^0 54.4′ is an artefact due to the remanence of the detector. The emission from the faint H II region N 4B is present, but below the displayed level. Contour levels are in mJy per square arc second. Compare to Fig. 1.

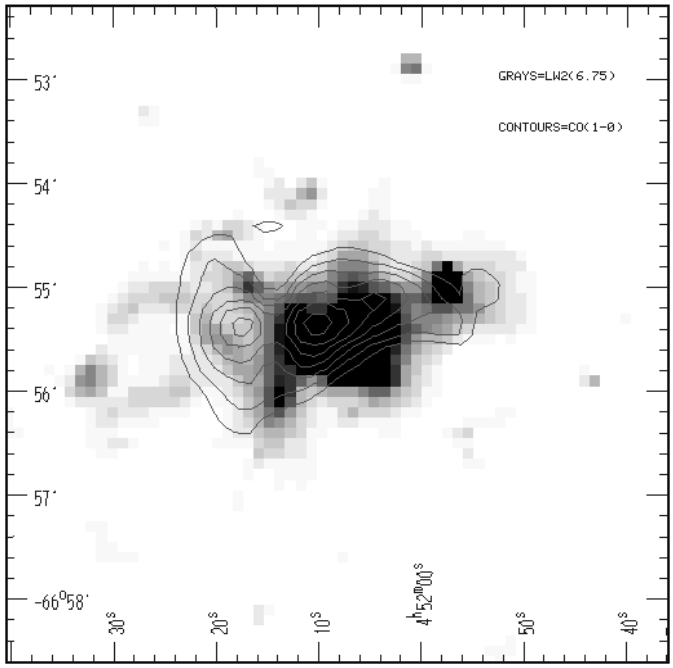

Fig. 3. CO(1–0) map of the N 4 region (contours) superimposed on the LW2 (6.75 μm) ISO image (gray scale). The coordinates are J2000. The CO map is from Heydari-Malayeri & Lecavelier des Etangs (1994) and has a 43″ resolution. The contour units are 2 to 8 in steps of 1 K km/s. The CO observations do not extend beyond the last displayed contour to the left of the figure.

ence of the point spread functions in the LW2 and LW3 filters (about 6″ and 8″ respectively) we convolved the image in the LW3 filter with the point spread function of the LW2 filter and vice versa. Actually, due to undersampling of the data the two products of convolution are not exactly the same. We might obtain a better result by downgrading images in both filters to a resolution of 2 pixels (12″) but at the expense of a further loss of reso lution.

The ratio map was then produced after clipping the convolved data to 3 times the r.m.s. noise as measured in empty fields of each convolved map. Due to uncertainties in calibration, in the background level and in the relative positioning of the two maps, the numerical values of the LW3/LW2 intensity ratio are uncertain where gradients exist and should be considered as indicative only. This ratio peaks on N 4A, where it reaches its maximum value of about 5, and also on N 4B (peak value about 3). In the region to the East of N 4A, far from the H II regions, the ratio is $\simeq$ 0.6–0.7.

Another presentation of the color data is given in Fig. 5. It displays the LW3/LW2 flux ratio profile obtained along a direction which passes through the exciting stars of N 4A and N 4B, as shown in Fig. 4. The enhancement of the ratio around these exciting stars is obvious.

We now compare the flux ratios observed in the region of N 4 with those in the Galaxy. In relatively quiet regions of the Galaxy, the LW3/LW2 flux ratio for pure PAHs is between 0.55 and 1.0 as estimated from the CAM-CVF spectra of NGC 7023 (Cesarsky et al. 1996a) and from the filter maps of the ρ Ophiuchi cloud obtained by Abergel et al. (1996). The values obtained to the east of N 4A, of the order of 0.6–0.7, are similar to the galactic values.

It is interesting to note that the ratio tends to be *lower* in regions submitted to a stronger radiation flux but not so strong as to yield a contribution of VSGs in the LW3 filter. This is for example the case for the brighter region in the map of the ρ Ophiuchi cloud which is illuminated by the B2V star HD 147889 (Abergel et al. 1996). On the other hand, the F(LW3)/F(LW2) ratio increases when the radiation field is very strong, due to the fact that the emission by VSGs becomes important in the LW3 filter. According to Cesarsky et al. (1996b) this occurs when the radiation density which excites the UIB emission is of the order of 10^4 times the density of the interstellar radiation field in the vicinity of the Sun: fields with such high densities exist inside H II regions or in their immediate vicinity. It is noticeable that although the outline of the UIB emission is similar to that of the CO one (Fig. 3) there is no correspondence between the CO and UIB emission peaks. Presumably the UIB emission comes from the external skin of the molecular complex whose internal structure is revealed by the CO map. The UIBs on this surface are excited by the general radiation field of this region of the LMC, except of course close to the H II region.

It is clear that the higher values of the F(LW3)/F(LW2) ratio near the H II regions N 4A and B are due to the contribution of VSGs to the flux around 15 μm. These grains are heated to

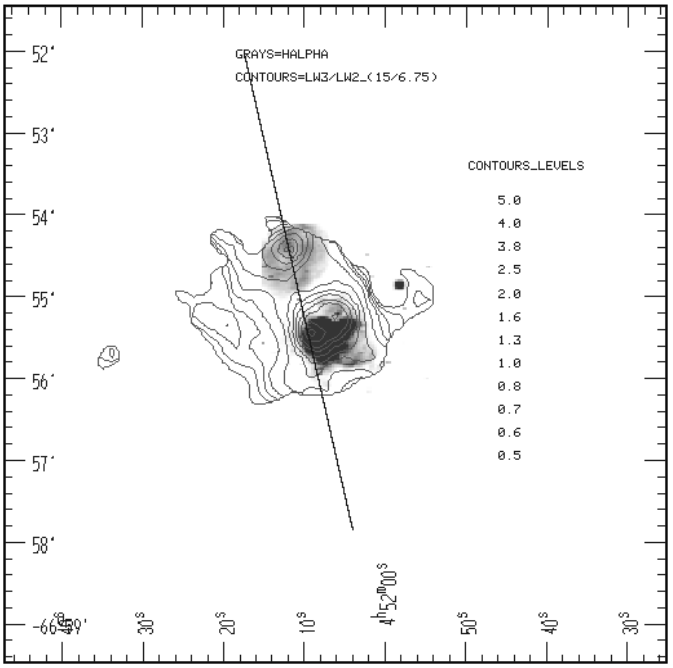

Fig. 4. Color map of the N 4 region displaying the F(LW3)/F(LW2) intensity ratio (contours) after smoothing to the same resolution, superimposed on an Hα image. The coordinates are J2000. The contour levels are rather uncertain, as explained in the text. Note the peaks on the two HII regions N 4A and B corresponding respectively to values $\simeq$ 4.5 and 3 of the ratio. The ratio for N 4B is particularly uncertain since the intensity of the source in the LW2 filter is at the limit of the 3 times r.m.s. noise level per pixel of the convolved image. The line through N 4A and N 4B corresponds to the cut displayed in Fig. 5.

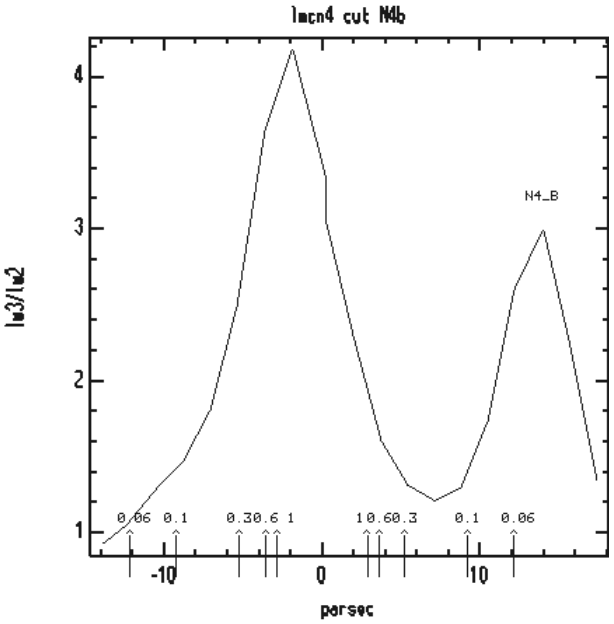

Fig. 5. Variations of the F(LW3)/F(LW2) flux ratio along a cut passing through the direction of the exciting stars of N 4A and N 4B (see Fig. 4). The scale of the abscissae is in parsec, and the arrows point to the estimated values of the UV radiation density due to N 4A (at 1600 Å) expressed in units of 10^4 times the interstellar radiation field in the vicinity of the Sun. These values have not been corrected for extinction and scattering and are upper limits. The values of the F(LW3)/F(LW2) ratios are rather uncertain, as explained in the text. The ratio for N 4B is particularly uncertain since the intensity of the source in the LW2 filter is at the limit of the 3 r.m.s. noise level per pixel of the convolved image. Note the peaks on the two HII regions N 4A and B corresponding respectively to values $\simeq$ 4.5 and 3 of this ratio.

temperatures sufficiently high for radiating at this wavelength, requiring a high UV flux as discussed previously. This flux is marginally reached near N 4C, but the flux near N 4B is clearly higher and that near N 4A considerably higher.

In order to be quantitative, we have estimated the far-UV radiation density at 1600 Å (a wavelength efficient for heating dust) around N 4A in the following way. The spectral type of the two exciting stars of N 4A, assumed identical, was determined to be O5V from the emitted flux of Lyman continuum photons (Panagia 1973), itself derived from the radio continuum flux with the relation given in Lequeux et al. (1981), after correction by a factor 2 to take into account the loss of such photons by dust absorption inside the H II region. The radio continuum data at 6 cm used in this determination can be found in Heydari-Malayeri & Lecavelier des Etangs (1994). Then the flux emitted by the stars at 1600 Å was estimated from the relations of Nandy et al. (1976), and the radiation density was computed as a function of the distance to the stars and normalized to the radiation density near the Sun taken from Gondhalekar et al. (1980). Extinction and scattering of the 1600 Å photons by dust have been neglected in view of our ignorance of the geometry of the dust distribution around N 4A, so that the estimated radiation density is an upper limit. This may not be too inaccurate in view of the fact that the region south of N 4A does not contain much matter, and the cut through the north passes through a minimum in the clumpy distribution of molecules in the interface H II region/molecular cloud, as can be seen on the ^{12}CO(2–1) map of Fig. 8b of Heydari-Malayeri & Lecavelier des Etangs (1994). The normalized radiation density at 1600 Å is indicated in the abscissae of Fig. 5 in units of 10^4. It appears that the 15 to 6.75 μm flux ratio becomes significantly higher than the ratio of 0.6–0.7 for quiet regions when the far-UV radiation density is higher than about 10^3 times that in the vicinity of the Sun. We cannot assess if this limit is the same as in our Galaxy or is different.

An analysis of N 4B and of its exciting star should allow us to determine the local radiation density and would be a welcome check of the above result. At any rate, it is interesting to note that there is dust (at least VSGs and probably UIB carriers) remaining inside this relatively faint H II region, which according to Heydari-Malayeri & Lecavelier des Etangs (1994) is older than N 4A.

Both the LW2 and LW3 filter maps show an intensity maximum displaced to the NE, on the edge of the H II region. This shows that most of the emission comes from the interface between the H II region and the molecular cloud, where the PAHs and VSGs are concentrated. This interface contains the compact H II region designated as α by Heydari-Malayeri & Lecavelier des Etangs (1994). It coincides with a secondary maximum

in the color map, while the main maximum almost coincides with the directions of the exciting stars: this shows that VSGs are probably also present in the H II region N 4A itself. This situation is very similar to that in the Galactic complex M17 (Cesarsky et al. 1996b), including the existence of a compact H II region in the interface which presumably represents the last stage of massive star formation in the complex.

5. Conclusions

From our broad-band ISO mapping of the region of N 4 in the LMC at 6.75 and 15 μm and comparison with Hα and CO(1–0) images, we derive the following conclusions.

i) The mid-IR emission far from the H II regions comes from UIBs excited by the general radiation field at the surface of the molecular cloud. The ratio of the 15 μm emission to that at 6.75 μm ($\simeq$0.6–0.7) is comparable to that found in quiet areas of our galaxy (0.55–1.0), suggesting similar properties for the UIB carriers. This however has to be checked by mid-IR spectroscopy which is presently programmed with ISO.

ii) The (15 μm)/(6.75 μm) flux ratio is considerably enhanced in regions of strong UV flux near the H II regions, as soon as the far-UV radiation density reaches approximately 10^3 times that in the vicinity of the Sun. This is due to the contribution of very small grains at 15 μm. These very small grains seem to survive inside H II regions as shown by the mid-IR emission from the centers of these H II regions.

iii) However the emissions at both wavelengths peak on an interface between the H II region N 4A and the molecular cloud. The situation in this region is very similar to that in the classical interface of M 17 in our Galaxy (Cesarsky et al. 1996b), including the presence of an ultra-compact H II region.

Acknowledgements. We are grateful to our referee, Dr. J. Guertler, for his constructive criticisms on a first version of this paper and to H. Aussel who made available to us the software to correct field distortion.

References

Abergel A., Bernard J.-P., Boulanger F. et al. 1996, A&A 315, L329
Cesarsky D., Lequeux J., Abergel A. et al. 1996a, A&A 315, L305
Cesarsky D., Lequeux J., Abergel A. et al. 1996b, A&A 315, L309
Davies R.D., Elliott K.H., Meaburn J. 1976, Mem. R. astr. Soc. 81, 89
Désert F.-X., Boulanger F., Puget J.-L. 1990, A&A 237, 215
Dwek E., Arendt R.G., Fixsen D.J. et al. 1997, ApJ 475, 565
Gondhalekar P.M., Phillips A.P., Wilson R. 1980, A&A 85, 272
Henize K.G. 1956, ApJS 2, 315
Heydari-Malayeri M., Lecavelier des Etangs A. 1994, A&A 291, 960
Lequeux J., Maucherat-Joubert M., Deharveng J.-M., Kunth D. 1981, A&A 103, 305
Nandy K., Thompson G.I., Jamar C., Monfils A., Wilson R. 1976, A&A 51, 63
Panagia N. 1973, AJ 78, 929
Rebeirot E., Martin N., Mianes P., Prévot L., Robin A., Rousseau J., Peyrin Y. 1983, A&AS 51, 277
Sauvage M., Thuan T.X., Vigroux L. 1990, A&A 237, 296
Westerlund B.E., Olander N., Hedin B. 1981, A&AS 43, 267